JACS
JOURNAL OF THE AMERICAN CHEMICAL SOCIETY
pubs.acs.org/JACS
Article

Force-Activated Isomerization of a Single Molecule

Jing Qi,[●] Yixuan Gao,[●] Haihong Jia, Marcus Richter, Li Huang, Yun Cao, Huan Yang, Qi Zheng, Reinhard Berger, Junzhi Liu, Xiao Lin, Hongliang Lu, Zhihai Cheng, Min Ouyang, Xinliang Feng,* Shixuan Du,* and Hong-Jun Gao*

Cite This: *J. Am. Chem. Soc.* 2020, 142, 10673−10680

ABSTRACT: Understanding and controlling isomerization at the single molecular level should provide new insight into the molecular dynamics and design guidelines of functional devices. Scanning tunneling microscopy (STM) has been demonstrated to be a powerful tool to study isomerization of single molecules on a substrate, by either electric field or inelastic electron tunneling mechanisms. A similar molecular isomerization process can in principle be induced by mechanical force; however, relevant study has remained elusive. Here, we demonstrate that isomerization of a *N*,*N*-dimethylamino-dianthryl-benzene molecule on Ag(100) can be mechanically driven by the STM tip. The existence of an out-of-plane dimethylamino group in the molecule is found to play a pivotal role in the isomerization process by providing a steric hindrance effect for asymmetric interaction between the STM tip and the molecule. This underlying mechanism is further confirmed by performing molecular dynamics simulations, which show agreement with experimental results. Our work opens the opportunity to manipulate the molecular configuration on the basis of mechanical force.

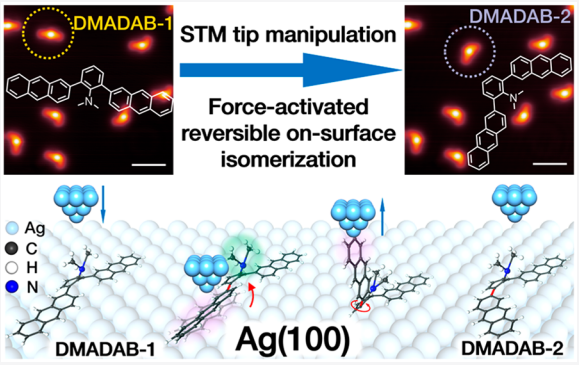

INTRODUCTION

Molecular isomers possessing subtle structural variations often manifest dramatic differences in physical and chemical properties.[1−4] Investigation on isomerization[5−7] can boost the research in enantioselective synthesis,[8−10] chiral catalysis,[6,11−13] and chiral pharmaceutical synthesis.[14,15] However, probing or even controlling the exact configuration of isomers at the single molecular level in solution has posed substantial challenges due to the three-dimensional rotation of isomers.[16] Recently, studying on-surface isomerization has offered an alternative route.[17−22] In this context, scanning probe microscopy (SPM) has been proved to be a powerful technique in relevant studies. In addition to its atomic spatial resolution,[19,23−25] the SPM can be utilized to manipulate molecules through different mechanisms,[26,27] making it an ideal tool to study isomerization at the single molecular level. Although mechanisms involving light and/or electrical activation have been investigated,[17,19,25,26,28−32] using mechanical force to induce isomerization has been relatively rare.[33−35]

Here, we have employed a scanning tunneling microscope (STM) tip to apply force interactions with *N*,*N*-dimethylamino-2,6-di(2-anthryl)-benzene (DMADAB) molecules on the Ag substrate to trigger its isomerization, which can be directly characterized by atomic imaging. The underlying mechanism uncovered by performing molecular dynamics simulations and a control experiment confirms that the out-of-plane dimethylamino group is essential for isomerization in this case.

RESULTS AND DISCUSSION

The synthesis of DMADAB was carried out in two steps starting from the commercially available 2,6-bromoaniline (see the Supporting Information). The DMADAB consists of a central benzene ring functionalized with an out-of-plane dimethylamino group and two anthryl groups at the *ortho*-positions. Because of the rotation of the two C−C bonds between the anthryl groups and the central benzene ring during sublimation, three isomers were formed on the substrate. Figure 1a is a large-area STM topographic image showing the three isomers of DMADAB after deposition, as marked by DMADAB-1, DMADAB-2, and DMADAB-3. Figure 1b−d shows the zoom-in STM images and the optimized structures of the three DMADAB isomers on the Ag(100) substrate. The two anthryl groups in DMADAB-1 are almost parallel, while in DMADAB-2 one anthryl group turns inward, forming an "L"-shaped configuration. Isomer DMADAB-3 has both anthryl groups turn inward, forming a "V"-shaped configuration. The angle between the two anthryl

Received: January 10, 2020
Published: May 27, 2020

https://dx.doi.org/10.1021/jacs.0c00192
J. Am. Chem. Soc. 2020, 142, 10673−10680

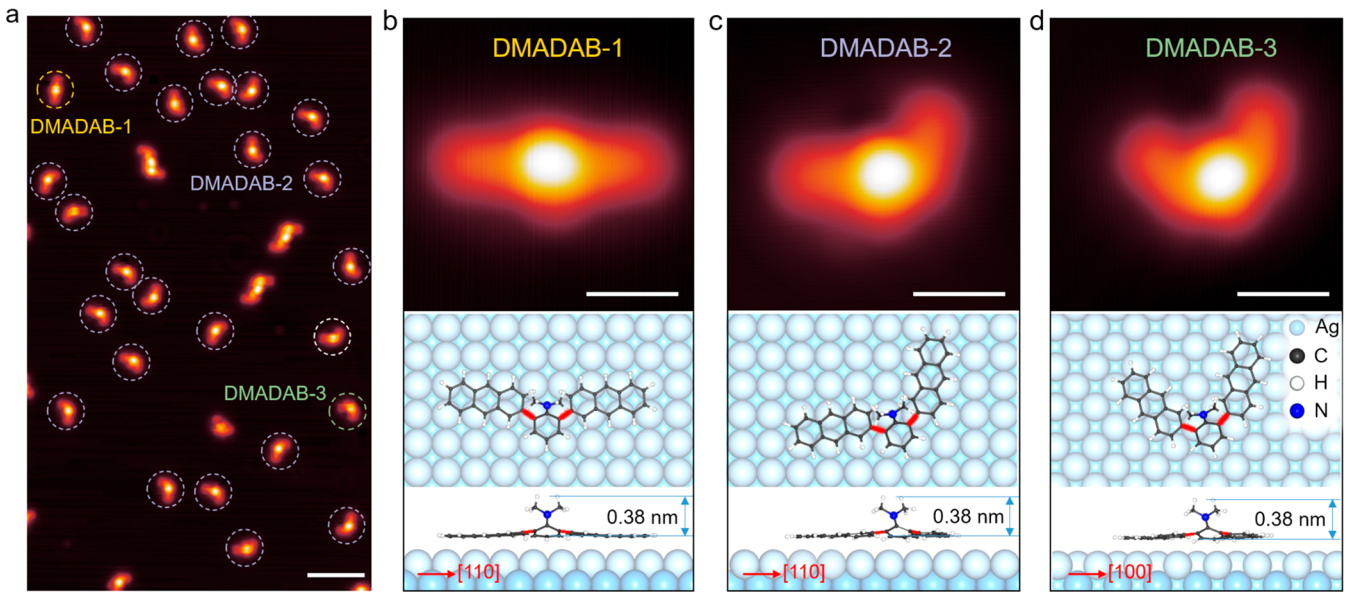

Figure 1. Isomers of DMADAB on the Ag(100) substrate. (a) 30 × 50 nm^2 STM topographic image of DMADAB after deposition at room temperature (rt). The three isomers are labeled in dashed circles with different colors (DMADAB-1, yellow; DMADAB-2, blue; and DMADAB-3, green). Scale bar: 5 nm. (b–d) STM topographic images, and top and front views of the DFT optimized structures of DMADAB-1, DMADAB-2, and DMADAB-3 on the Ag(100) substrate, respectively. The C–C bonds in red in the lower panels indicate the rotatable C–C bonds. The red arrows indicate the crystal orientations of the substrate. Scanning parameters are V_{sample} = −100 mV and I = 30 pA. Scale bars: 1 nm.

groups in a DMADAB molecule is used as a criterion to classify the three isomers, as depicted in Figure S1. In the STM topographic images in the upper panels of Figure 1b–d, the three DMADAB isomers show bright protrusions in the middle due to the out-of-plane dimethylamino groups. The lower panels of Figure 1b–d are the top and side views of the most stable configurations of the DMADAB isomers on the Ag(100) surface obtained by density functional theory (DFT) calculations. To exclude other configurations, we also intentionally used a configuration in which both of the anthryl groups are standing on the surface as the initial structure in DFT calculation, and the anthryl groups lie flat on the substrate after structural relaxation (Figure S2), which confirms the configurations in Figure 1b–d are the most energetically favorable ones. The side view of the isomers on the substrate displays that the topmost hydrogen atom of the protuberant methyl groups is about 0.38 nm higher than the average plane of the two anthryl groups.

The DFT calculated adsorption energies are −3.192, −3.327, and −3.355 eV, for DMADAB-1, DMADAB-2, and DMADAB-3 on Ag(100), respectively. It means that we should observe more DMADAB-3 on the Ag(100) substrate. However, from the STM image (Figure 1a) and the quantitative populations for these three isomers (Figure S1c), we found that there are more DMADAB-2 isomers than others. To explain this, we optimized the structures of the DMADAB isomers in a vacuum and calculated their total energies relative to DMADAB-1 (Figure S3). The respective total energies of DMADAB-2 and DMADAB-3 are 0.035 and 0.066 eV higher than that of DMADAB-1, suggesting that DMADAB-1 is the dominant isomer in a vacuum before landing on the surface. The adsorption energy determines which isomer is easier to adsorb on the surface, while the total energy in a vacuum determines the initial quantities of each isomer. DMADAB-1 has the largest initial quantity but is the hardest to adsorb on the surface, while DMADAB-3 is the easiest to adsorb on the surface but has the smallest initial quantity. The competition between the two factors results in DMADAB-2, which has medium adsorption energy and total energy in vacuum, becoming the most favorable isomer on the Ag(100) surface.

We performed STM tip manipulation on the isomers to investigate their on-surface isomerization. The manipulations were done by opening the feedback loop, decreasing the bias voltage to zero, approaching the STM tip to the target isomer, and then lifting the tip up (Figure 2a). Figure 2b–f demonstrates manipulations on one DMADAB molecule (as indicated by dashed circles) that trigger the transitions between isomers. Isomer DMADAB-1 in Figure 2a had one of its anthryl groups (marked with a green ellipse) rotated upon manipulation, which resulted in DMADAB-2 (Figure 2b,c). Further manipulation on the isomer DMADAB-2 made the other anthryl group rotate and isomerize to DMADAB-3 (Figure 2c,d). This process is reversed, as shown in Figure 2d, when DMADAB-3 was manipulated, as one anthryl group rotated and turned to DMADAB-2 (Figure 2d,e). Further manipulation made the other anthryl group rotate and turn to DMADAB-1 (Figure 2e,f). We have performed 223 manipulations on DMADAB molecules, and the overall success rate was 28.7%, as shown in the statistics in Figure 2g. We did not observe the direct isomerization between DMADAB-1 and DMADAB-3, which involves the rotation of both anthryl groups and indicates a large energy barrier of rotating both anthryl groups simultaneously. Meanwhile, from the statistics in Figure 2g, the successful isomerization rates for DMADAB-1 to DMADAB-2, DMADAB-2 to DMADAB-1/3, and DMADAB-3 to DMADAB-2 are comparable, which suggests comparable energy barriers of rotating one anthryl group in all three isomers.

With the support of steered molecular dynamics (SMD) simulations, we tried to elucidate the mechanism behind the isomerization of DMADABs. Taking the isomerization process

https://dx.doi.org/10.1021/jacs.0c00192
J. Am. Chem. Soc. 2020, 142, 10673−10680

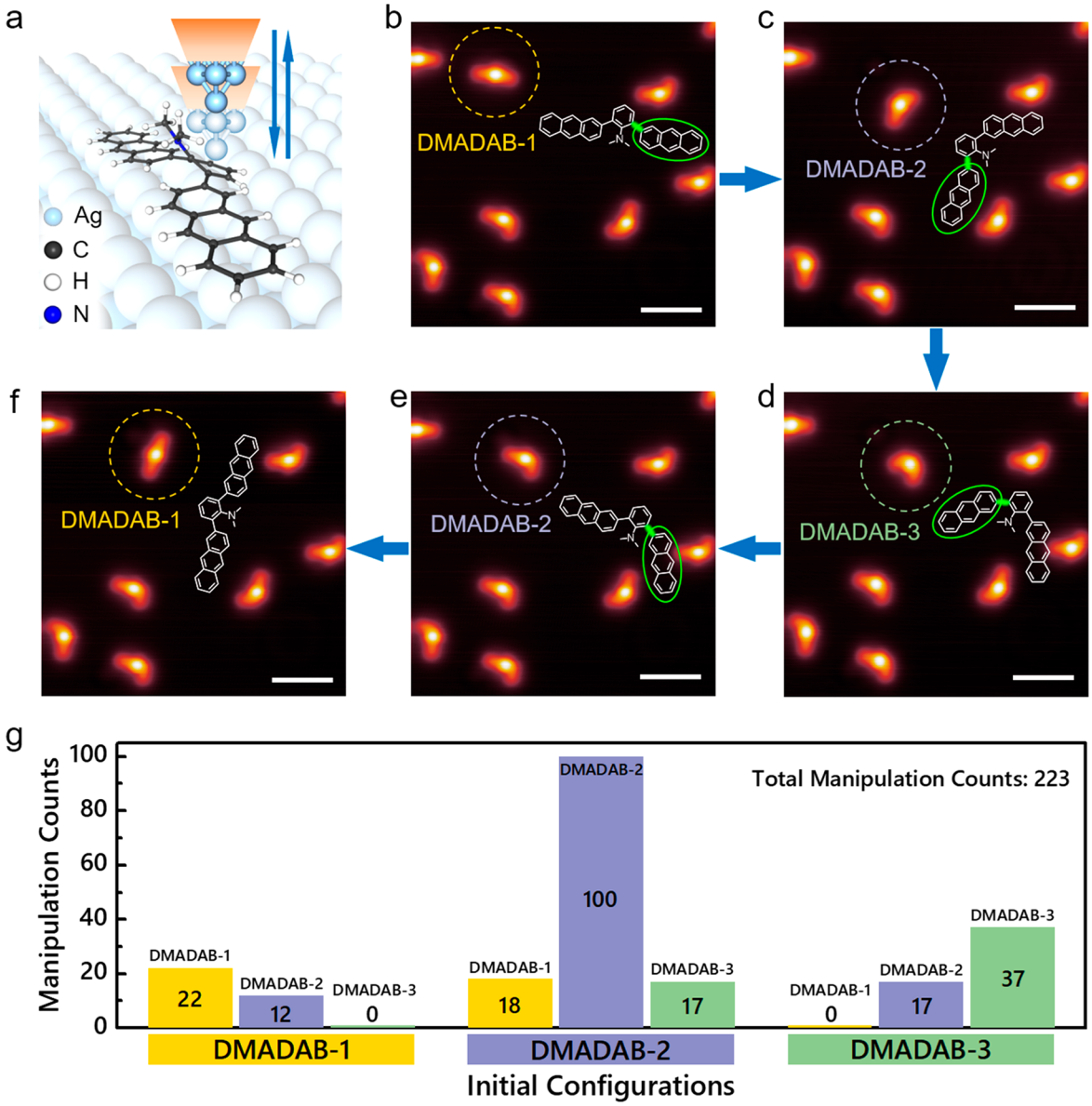

Figure 2. Reversible isomerization of DMADAB on the Ag(100) surface by STM tip manipulation. (a) Schematic of the tip vertical manipulation. The tip approaches to the target DMADAB isomer and then retracts, which causes the transition. (b–f) STM images show STM tip manipulation-induced isomerization on the same DMADAB molecule on the Ag(100) substrate. The images are in time order, but not consecutive. Some images with the same configurations are omitted. The dashed circles indicate the isomers being manipulated. Reversible isomerization between all three isomers of DMADAB has been achieved. The corresponding molecular structures are depicted in the images, in which the bonds marked green highlight the rotated C–C bond and the green ellipses highlight the rotating anthryl groups. Scanning parameters are $V_{sample} = -100$ mV and $I = 30$ pA. Scale bars: 2 nm. (g) Statistics of tip manipulations on DMADAB isomers. The overall success rate of isomerization is 28.7% in 223 manipulations.

from DMADAB-1 to DMADAB-2 as an example, the simulated movie demonstrates the process starting from the tip (metal apex, no carbon monoxide functionalized) approaching to the molecule and ending with the tip retracting (see movie S1 and snapshots in Figure S4). The four typical states from the simulation are depicted in Figure 3. First, the tip is approaching on a DMADAB-1 isomer on the Ag(100) substrate. When the tip is far away from the molecule, the DMADAB-1 keeps its original adsorption configuration with its two anthryl groups aligned parallel to the substrate and the dimethylamino group pointed straight upward, as indicated in Figure 3a. When the tip approaches to the surface, the DMADAB-1 isomer moves toward the tip. Because of the repulsive force induced by the out-of-plane dimethylamino group (marked by a green halo), one of its anthryl groups goes closer to the tip and rotates to have an attractive force with the tip, as shown by the purple halo and red arrow in Figure 3b. Afterward, when the tip retracts from the substrate, the strong interaction from the tip pulls up the rotated anthryl group along with the central benzene ring (Figure 3c). However, with the other anthryl group still adsorbing on the substrate, the molecule detaches from the tip when the tip further retracts and falls on the surface with one of the anthryl groups completely rotated to isomer DMADAB-2 (Figure 3d). Furthermore, the SMD simulations also show that the rotation direction of the anthryl group is outward, that is, away from the

https://dx.doi.org/10.1021/jacs.0c00192
J. Am. Chem. Soc. 2020, 142, 10673–10680

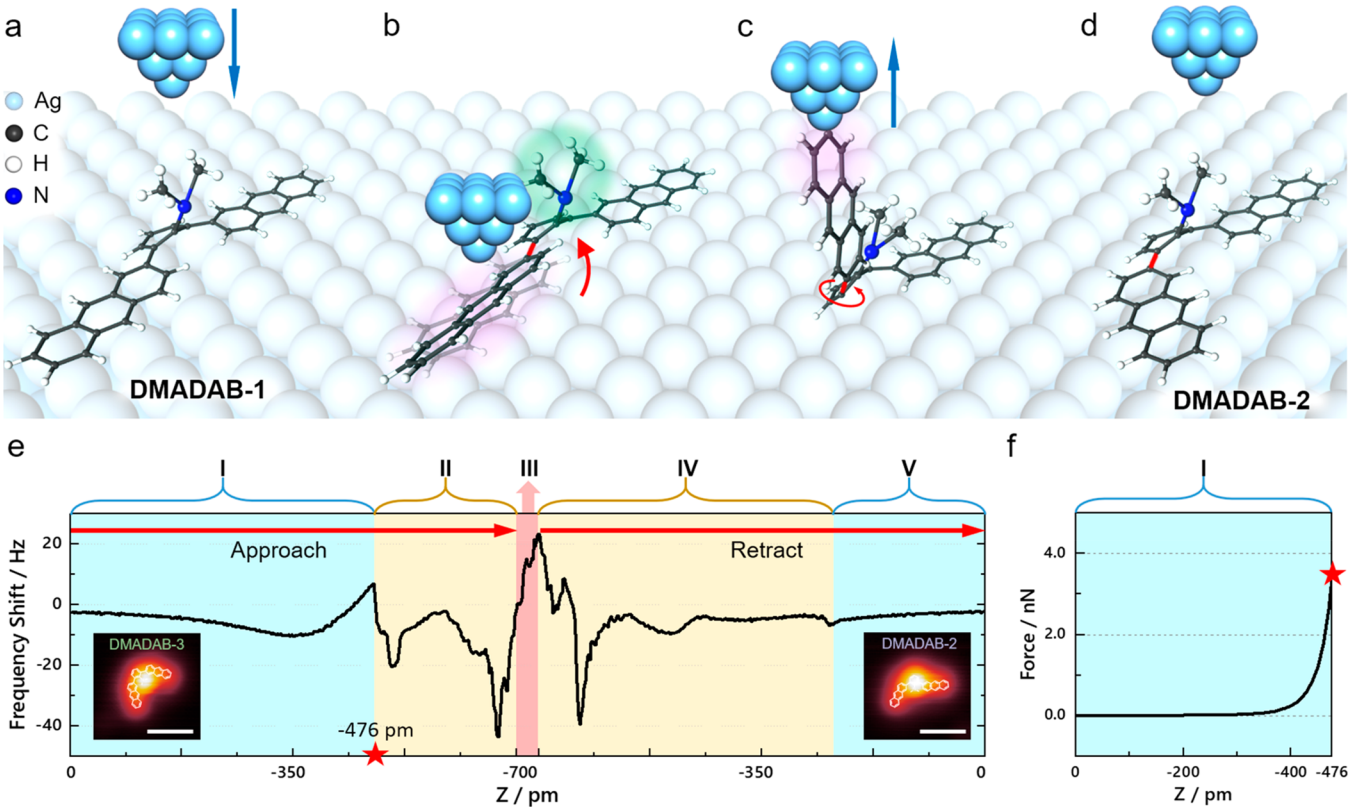

Figure 3. Four typical states in tip manipulation on DMADAB taken from the SMD simulations and the $\Delta f(Z)$ curve on a successful isomerization. (a) The tip is approaching a DMADAB-1. (b) When the tip is close to the DMADAB-1, the out-of-plane dimethylamino group (in green halo) gives the tip a repulsive force, which induces the tip to go to one side of the molecule and have attractive force with one of the anthryl groups (in purple halo). As a result, the anthryl group rotates as indicated by the red arrow. (c) When the tip retracts, the anthryl group and the central benzene ring are lifted up by the tip, with the other anthryl group still lies on the substrate. (d) When the tip further retracts, the contact of the anthryl group and the tip breaks, and the anthryl group rotates completely when it falls back to the substrate and transits to DMADAB-2. (e) The $\Delta f(Z)$ curve recorded during a successful manipulation on a DMADAB molecule. Insets are STM images of the DMADAB molecule before (left) and after (right) manipulation. Scale bars are 1 nm. Z = 0 pm is defined as a tunneling junction height of −300 mV, 10 pA on top of the dimethylamino group. Regions I and II correspond to the tip approaching to the molecule from 0 to −700 pm. Region III is where the tip stays at −700 pm for 3 s. Regions IV and V correspond to the tip retracting from −700 to 0 pm. The feedback loop was open during the $\Delta f(Z)$ measurements. (f) The short-range force curve calculated from the $\Delta f(Z)$ curve in region I. The red star marks the Z position at −476 pm, where $\Delta f(Z)$ suddenly drops at the boundary of regions I and II. The force curve is calculated via the Sader−Jarvis method.[36]

dimethylamino group, due to the steric hindrance (Figure S5a-f).

We have recorded the curves of frequency shift (Δf) versus tip−molecule distance (Z) of successful manipulations on DMADAB molecules (Figures 3e and S6). As shown in Figure 3e, the $\Delta f(Z)$ curve in regions I and II displays the tip−molecule interaction when the tip approached to the molecule for 700 pm from a tunneling junction height of −300 mV, 10 pA, where Z is defined as 0 pm. In region I, the curve features the Lennard-Jones force law, and the corresponding short-range force curve is calculated and displayed in Figure 3f, which indicates that the force between the tip and the molecule is a repulsive force of 3.38 nN at −476 pm. When further approaching the tip, the frequency shift suddenly drops at −476 pm and then undergoes a drastic changes in region II. This sudden drop, which is defined as the "bonding point", is attributed to the involvement of nonconservative processes between the tip and the molecule, such as the formation of chemical bonds. For different manipulations, the bonding points in $\Delta f(Z)$ vary around an average value of −492 ± 30 pm (Figure S6). In region III, the tip stayed at −700 pm for 3 s, where the frequency shift may change, which suggests unstable structures under the tip. The $\Delta f(Z)$ curve with tip retraction is displayed in regions IV and V. In region IV, the frequency shift shows large variations, which should correspond to the lifting of one of the anthryl groups by the tip along with cleavages of the bonds that were formed in region II. Further retracting from −243 to 0 pm, the $\Delta f(Z)$ curve monotonically increases, which suggests the anthryl group has detached from the tip at −243 pm. Note that the detachment of the anthryl group may also happen at 0 pm or even higher tip positions (Figure S6). Given the complex interactions involved in the process, the change of the detachment height is reasonable. The deduced isomerization process from the $\Delta f(Z)$ curves fits well with the SMD simulations. In this whole process, the dimethylamino group plays a key role in inducing the molecule to interact with the tip with one of its anthryl groups by providing a repulsive force in the middle part of the molecule. It is predictable that without this out-of-plane dimethylamino group, the molecule and tip are likely to interact at the central benzene ring, which makes the isomerization unlikely to happen.

To concrete the role of the dimethylamino group in isomerization, we removed the dimethylamino group in DMADABs by annealing the substrate at 670 K for 40 min, which converted all DMADABs to 1,3-di(2-anthryl)-benzene (DAB) species. The DABs have three isomers on the surface as

https://dx.doi.org/10.1021/jacs.0c00192
J. Am. Chem. Soc. 2020, 142, 10673−10680

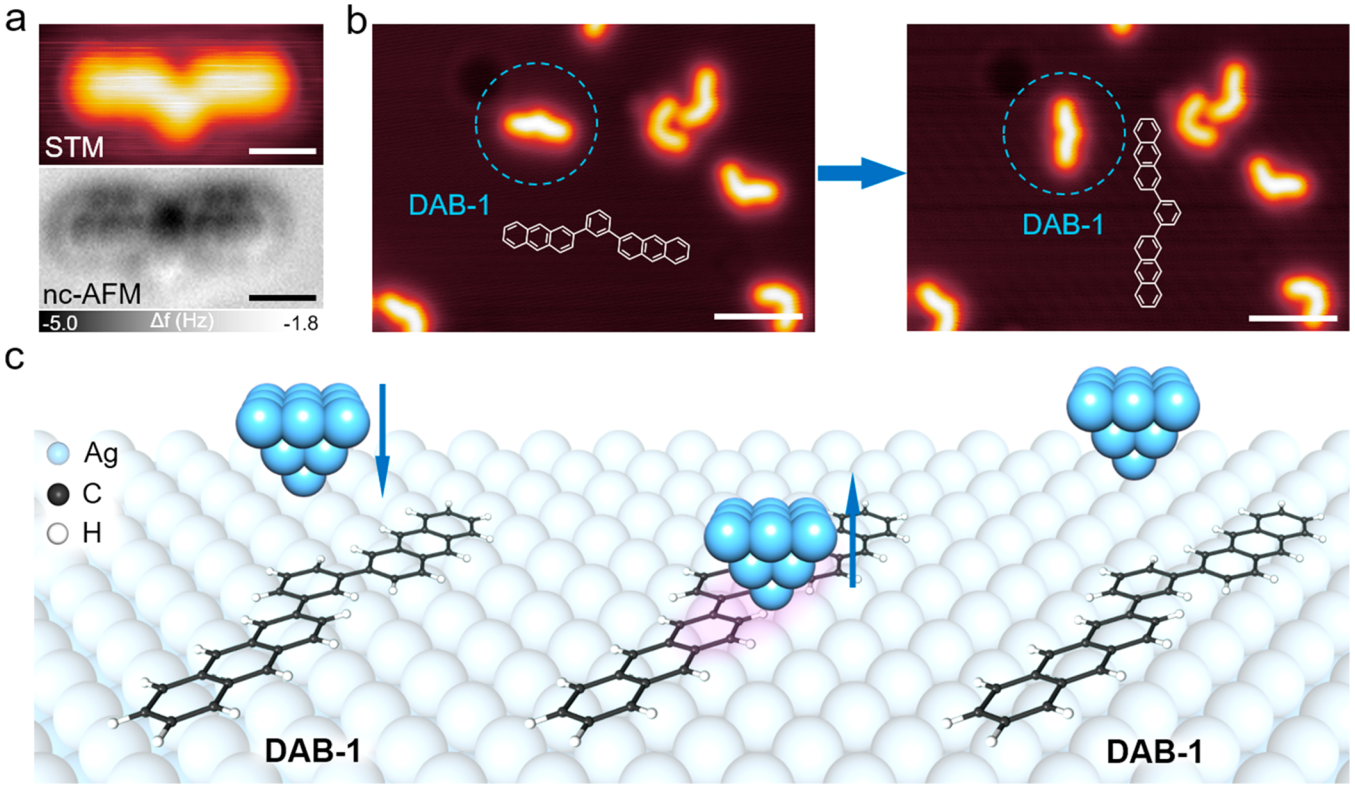

Figure 4. Control experiment on DAB molecule on Ag(100). (a) STM topographic images and constant-height frequency shift nc-AFM images of DAB-1 on the Ag(100) substrate. STM scanning parameters: V_{sample} = −30 mV and I = 10 pA. AFM scanning parameters: amplitude = 100 pm. Scale bars: 1 nm. (b) Continuous tip manipulation of DAB-1 shows that DAB-1 can move around and rotate, but not transit to another isomer. Dashed circles indicate the molecule being manipulated. Scanning parameters: V_{sample} = −100 mV and I = 10 pA. Scale bars: 3 nm. (c) Schematic drawing of the typical states in tip manipulation on DAB-1 taken from the SMD simulations. The tip interacts with the central region of the molecule (in purple halo) after approaching to the substrate. Thus, none of the anthryl groups rotate in the manipulation process, and no transition can be triggered.

counterparts of the DMADAB isomers. Similar to DMADAB, the angle between the two anthryl groups in a DAB molecule is used as a criterion to classify the three isomers (Figure S1). Figure 4a shows the STM and noncontact atomic force microscope (nc-AFM) images of a DAB-1 molecule, which yields unambiguous evidence for the detachment of the dimethylamino group and leaves two anthryl groups intact at the *meta*-position of the central benzene ring and results in a planar configuration. The STM and nc-AFM images of DAB-2 and DAB-3 also show similar planar configurations (see Figure S7). The nc-AFM images show a hexagon feature at the center with two neighboring anthryl groups, which is in good agreement with the planar configuration of DAB molecules. The planar configuration is distinct from those of the DMADAB isomers. The nc-AFM images of DMADAB-2 (Figure S8) with decreasing tip heights clearly resolve an out-of-plane group. The disappearance of the out-of-plane group in DAB nc-AFM images is strong evidence for the detachment of the dimethylamino group after annealing. For comparison, experimental and DFT simulated STM images for DMADABs and DABs are shown in Figures S9 and S10. The simulated DMADAB images all have a bright protrusion in the center, which corresponds to the dimethylamino group, and flat arms on both sides, which are the anthryl groups. For the DAB molecules, the simulated images show flat electronic states along the molecular skeleton. All of the simulated images fit well with our STM images.

The STM tip manipulation was also performed to investigate the isomerization behavior of DAB isomers. However, with multiple combinations of manipulation heights and rates, only lateral displacement but no isomerization was observed (DAB-1 in Figure 4b and DAB-2, DAB-3 in Figure S11, respectively). Of all of the 147 trials that we have performed on DAB molecules, no isomerization was induced (the statistics is shown in Figure S12). This result demonstrates that without the out-of-plane dimethylamino group, the isomerization is blocked, although the force between the tip and the molecule is large enough to move the molecule on the surface.

In the SMD simulated movie (see movie S2), DAB-1 shows a dramatic difference from DMADABs upon tip manipulation. First, the molecule has a planar adsorption configuration on the substrate. As the tip approaches the surface, the DAB-1 moves toward the tip with its middle region (purple halo in Figure 4c) directly interacting with the tip. The molecule remains in the planar configuration during the manipulation process, which thus makes it rather unlikely for either of the anthryl groups to rotate. When the tip retracts, the molecule either stays on the surface with its original configuration or is picked up by the tip. From this control experiment on the manipulation of molecules without dimethylamino groups, we have confirmed that the repulsive force interaction between the tip and the out-of-plane dimethylamino group is essential for isomerization of DMADABs.

https://dx.doi.org/10.1021/jacs.0c00192
J. Am. Chem. Soc. 2020, 142, 10673−10680

CONCLUSION

We studied isomerization for DMADABs by STM tip manipulation on the Ag(100) substrate. The DMADABs can reversibly and reproducibly isomerize between three configurations. The SMD simulations demonstrate that the repulsive force between the tip and the out-of-plane dimethylamino group is essential for the isomerization. After detachment of the dimethylamino group, the resulting planar molecules DAB no longer change their configurations upon tip manipulation. Our work demonstrates that it is feasible to use out-of-plane functional groups to tune on-surface molecular isomerization and opens the possibility to manipulate molecular configurations via mechanical forces.

EXPERIMENTAL METHODS

Sample Preparation. Synthesis method and characterization data for DMADAB molecule are supplied in the Supporting Information. Experiments were done in an ultrahigh vacuum (UHV) chamber with the base pressure of 2×10^{-10} mbar. The Ag(100) surface was prepared by repeated cycles of Ar^+ ion sputtering and annealing to 660 K for 20 min. The DMADAB was sublimed onto a clean Ag(100) surface at 470 K for 3 min while keeping the substrate at rt, allowing possible on-surface isomerization to happen. Full deamination of DADBAMs was done by annealing the substrate to 670 K for 40 min.

SPM Measurements. All STM and nc-AFM measurements were performed at LHe temperature with the base pressure lower than 2×10^{-10} mbar. All STM topographic images were acquired in constant-current mode. All nc-AFM measurements were performed using a commercial qPlus tuning fork sensor in frequency modulation mode with a carbon monoxide (CO)-functionalized Pt/Ir tip.[37] The resonance frequency is about 27.9 kHz, and the stiffness is about 1800 N/m. The imaging heights for all nc-AFM measurements as reported in the figure captions referred to the STM tunneling junction height on a clean Ag(100) substrate, which is −30 mV and 10 pA. All STM and nc-AFM images were processed using the free and open source software Gwyddion.

STM Tip Manipulation. We first scan the sample to make sure the tip is not decorated with molecules. The tip is clean if the shape of molecule can be clearly resolved in STM images. Tip manipulation was done by stabilizing the STM tip on the Ag(100) surface after some certain time. Afterward, we move the tip to the center of the target molecule, open the feedback loop, subsequently decrease the bias to zero, and approach the tip to the target molecule for a certain distance before retracting the tip. The STM feedback loop was then turned back on, and the STM scan was performed subsequently to confirm the result after each manipulation. For most of the manipulations, when opening the feedback loop, the tunneling junction was at a tunneling bias of −100 mV and a tunneling current of 30 pA, and the approaching distance was about 550 pm for around 60 ms before the tip was retracted by 1 nm. A tunneling junction height of −300 mV, 10 pA was also tried, for which the approaching distance for activating the isomerization was about 700 pm. At other initial heights, the isomerization can also be activated at a proper approaching distance.

THEORETICAL METHODS

SMD Simulations. The SMD simulations using the constant-velocity method are employed to study the effects of the STM tip on the rotation of molecules on the Ag(100) surface. We first construct a model consisting of a DMADAB/DAB molecule absorbed on a (30 × 30) lateral periodicity of the four-layered Ag(100) slab. The dimension of the supercell is 86.7 × 86.7 × 66.1 $Å^3$. The STM tip composed of 113 Pt atoms and 4 Ag atoms hangs over the substrate. The vertical external forces then are applied to the STM tip for simulating the approaching and withdrawing effect of the tip, respectively. All constant-velocity SMD simulations are performed with the pulling velocities of 0.01 nm/ps and loading rates of 16.61 pN/ps. All SMD simulations are conducted using the GROMACS 2016 simulation package.[38] The general AMBER force field (GAFF) is used to describe the inter- and intramolecular interaction parameters of the DMADAB/DAB molecule.[39,40] For Ag and Pt atoms, the Lennard-Jones (LJ) potential is chosen because it is compatible with the AMBER force field and its performance is comparable to that of tight-binding and embedded atom models.[41] The simulations are carried out with three-dimensional periodic boundary conditions using the leapfrog integrator with a time step of 1.0 fs. Short-range electrostatic and van der Waals interactions are calculated at a cutoff distance of 1.2 nm, whereas long-range electrostatic interactions are treated using the particle mesh Ewald method. The Berendsen thermostat is chosen for temperature. Simulation snapshots are rendered in visual molecular dynamics.[42]

DFT Calculations. All DFT calculations were carried out using the Vienna ab initio simulation package (VASP)[43] with the projector augmented wave (PAW) method.[44,45] The van der Waals (vdW) interactions were considered at the vdW-DF level,[46] with the optB86 functional used for the exchange potential.[47,48] The energy cutoff of the plane-wave basis sets was 400 eV, and K-point sampling was done only at the Γ point. A slab model was used with three Ag layers as the substrate. The vacuum layer was larger than 1.2 nm. All atoms except for the bottom Ag layer were fully relaxed until the net force was smaller than 0.1 eV/nm.

ASSOCIATED CONTENT

Supporting Information

The Supporting Information is available free of charge at https://pubs.acs.org/doi/10.1021/jacs.0c00192.

Synthesis and characterization of DMADAB, supplementary figures, and additional references (PDF)

Movie S1: SMD simulations on DMADAB-1 (MP4)

Movie S2: SMD simulations on DAB-1 (MP4)

AUTHOR INFORMATION

Corresponding Authors

Xinliang Feng − *Center for Advancing Electronics Dresden (cfaed) and Department of Chemistry and Food Chemistry, Technische Universität Dresden, Dresden 01069, Germany; School of Chemistry and Chemical Engineering, Shanghai Jiao Tong University, Shanghai 200240, China;* orcid.org/0000-0003-3885-2703; Email: xinliang.feng@tu-dresden.de

Shixuan Du − *Institute of Physics and University of Chinese Academy of Sciences, Chinese Academy of Sciences, Beijing 100190, China;* orcid.org/0000-0001-9323-1307; Email: sxdu@iphy.ac.cn

Hong-Jun Gao − *Institute of Physics and University of Chinese Academy of Sciences, Chinese Academy of Sciences, Beijing 100190, China;* orcid.org/0000-0002-6766-0623; Email: hjgao@iphy.ac.cn

Authors

Jing Qi − *Institute of Physics and University of Chinese Academy of Sciences, Chinese Academy of Sciences, Beijing 100190, China;* orcid.org/0000-0001-6859-750X

Yixuan Gao − *Institute of Physics and University of Chinese Academy of Sciences, Chinese Academy of Sciences, Beijing 100190, China*

Haihong Jia − *Institute of Physics and University of Chinese Academy of Sciences, Chinese Academy of Sciences, Beijing 100190, China*

Marcus Richter − *Center for Advancing Electronics Dresden (cfaed) and Department of Chemistry and Food Chemistry, Technische Universität Dresden, Dresden 01069, Germany*

Li Huang − *Institute of Physics and University of Chinese Academy of Sciences, Chinese Academy of Sciences, Beijing 100190, China*
Yun Cao − *Institute of Physics and University of Chinese Academy of Sciences, Chinese Academy of Sciences, Beijing 100190, China;* orcid.org/0000-0002-7518-2481
Huan Yang − *Institute of Physics and University of Chinese Academy of Sciences, Chinese Academy of Sciences, Beijing 100190, China*
Qi Zheng − *Institute of Physics and University of Chinese Academy of Sciences, Chinese Academy of Sciences, Beijing 100190, China*
Reinhard Berger − *Center for Advancing Electronics Dresden (cfaed) and Department of Chemistry and Food Chemistry, Technische Universität Dresden, Dresden 01069, Germany;* orcid.org/0000-0002-8959-7821
Junzhi Liu − *Center for Advancing Electronics Dresden (cfaed) and Department of Chemistry and Food Chemistry, Technische Universität Dresden, Dresden 01069, Germany;* orcid.org/0000-0001-7146-0942
Xiao Lin − *Institute of Physics and University of Chinese Academy of Sciences, Chinese Academy of Sciences, Beijing 100190, China*
Hongliang Lu − *Institute of Physics and University of Chinese Academy of Sciences, Chinese Academy of Sciences, Beijing 100190, China*
Zhihai Cheng − *Department of Physics and Beijing Key Laboratory of Optoelectronic Functional Materials & Micro-nano Devices, Renmin University of China, Beijing 100872, China;* orcid.org/0000-0003-4938-4490
Min Ouyang − *Department of Physics and Center for Nanophysics and Advanced Materials, University of Maryland, College Park, Maryland 20742, United States;* orcid.org/0000-0002-1721-1571

Complete contact information is available at: https://pubs.acs.org/10.1021/jacs.0c00192

Author Contributions

●J.Q. and Y.G. contributed equally to this work.

Notes

The authors declare no competing financial interest.

■ ACKNOWLEDGMENTS

We acknowledge the financial support from the National Key Research and Development Program of China (Grant nos. 2016YFA0202300, 2018YFA0305800, and 2016YFA0200700), the National Natural Science Foundation of China (Grant nos. 51761135130, 61888102, 61622116, 11604373, 21661132006, 21622304, 61674045, and 11604063), the Strategic Priority Research Program of the Chinese Academy of Sciences (Grant no. XDB30000000), the International Partnership Program of the Chinese Academy of Sciences (Grant no. 112111KYSB20160061), and the CAS Pioneer Hundred Talents Program. Furthermore, we thank the German Research Foundation (DFG) with EnhanceNano (no. 391979941) for financial support. Part of this research was performed in the Key Laboratory of Vacuum Physics, Chinese Academy of Sciences. Computational resources were provided by the National Supercomputing Center in the Tianjin Municipality, China.

■ REFERENCES

(1) Rando, R. R. The Chemistry of Vitamin-a and Vision. *Angew. Chem., Int. Ed. Engl.* **1990**, *29* (5), 461−480.
(2) Lummis, S. C. R.; Beene, D. L.; Lee, L. W.; Lester, H. A.; Broadhurst, R. W.; Dougherty, D. A. Cis-trans isomerization at a proline opens the pore of a neurotransmitter-gated ion channel. *Nature* **2005**, *438* (7065), 248−252.
(3) Liljeroth, P.; Repp, J.; Meyer, G. Current-induced hydrogen tautomerization and conductance switching of naphthalocyanine molecules. *Science* **2007**, *317* (5842), 1203−1206.
(4) Crespi, S.; Simeth, N. A.; Koinig, B. Heteroaryl azo dyes as molecular photoswitches. *Nat. Rev. Chem.* **2019**, *3* (3), 133−146.
(5) Garay, A. S. Molecular Chirality of Life and Intrinsic Chirality of Matter. *Nature* **1978**, *271* (5641), 186−186.
(6) Barrett, K. T.; Metrano, A. J.; Rablen, P. R.; Miller, S. J. Spontaneous transfer of chirality in an atropisomerically enriched two-axis system. *Nature* **2014**, *509* (7498), 71−75.
(7) Canfield, P. J.; Blake, I. M.; Cai, Z. L.; Luck, I. J.; Krausz, E.; Kobayashi, R.; Reimers, J. R.; Crossley, M. J. A new fundamental type of conformational isomerism. *Nat. Chem.* **2018**, *10* (6), 615−624.
(8) Liu, H. J.; Leow, D.; Huang, K. W.; Tan, C. H. Enantioselective Synthesis of Chiral Allenoates by Guanidine-Catalyzed Isomerization of 3-Alkynoates. *J. Am. Chem. Soc.* **2009**, *131* (21), 7212.
(9) Silverio, D. L.; Torker, S.; Pilyugina, T.; Vieira, E. M.; Snapper, M. L.; Haeffner, F.; Hoveyda, A. H. Simple organic molecules as catalysts for enantioselective synthesis of amines and alcohols. *Nature* **2013**, *494* (7436), 216−221.
(10) Storch, G.; Trapp, O. By-design enantioselective self-amplification based on non-covalent product-catalyst interactions. *Nat. Chem.* **2017**, *9* (2), 179−187.
(11) Behenna, D. C.; Liu, Y. Y.; Yurino, T.; Kim, J.; White, D. E.; Virgil, S. C.; Stoltz, B. M. Enantioselective construction of quaternary N-heterocycles by palladium-catalysed decarboxylative allylic alkylation of lactams. *Nat. Chem.* **2012**, *4* (2), 130−133.
(12) Phipps, R. J.; Hamilton, G. L.; Toste, F. D. The progression of chiral anions from concepts to applications in asymmetric catalysis. *Nat. Chem.* **2012**, *4* (8), 603−14.
(13) Chen, X.; Cheng, Z. Y.; Guo, J.; Lu, Z. Asymmetric remote C-H borylation of internal alkenes via alkene isomerization. *Nat. Commun.* **2018**, *9* (1), 1−8.
(14) Patel, R. N. Microbial/enzymatic synthesis of chiral intermediates for pharmaceuticals. *Enzyme Microb. Technol.* **2002**, *31* (6), 804−826.
(15) Patel, R. N. Synthesis of chiral pharmaceutical intermediates by biocatalysis. *Coord. Chem. Rev.* **2008**, *252* (5−7), 659−701.
(16) Lansac, Y.; Glaser, M. A.; Clark, N. A.; Lavrentovich, O. D. Photocontrolled nanophase segregation in a liquid-crystal solvent. *Nature* **1999**, *398* (6722), 54−57.
(17) Morgenstern, K. Isomerization Reactions on Single Adsorbed Molecules. *Acc. Chem. Res.* **2009**, *42* (2), 213−223.
(18) Riedel, D.; Cranney, M.; Martin, M.; Guillory, R.; Dujardin, G.; Dubois, M.; Sonnet, P. Surf ace-Isomerization Dynamics of trans-Stilbene Molecules Adsorbed on Si(100)-2 × 1. *J. Am. Chem. Soc.* **2009**, *131* (15), 5414−5423.
(19) Safiei, A.; Henzl, J.; Morgenstern, K. Isomerization of an azobenzene derivative on a thin insulating layer by inelastically tunneling electrons. *Phys. Rev. Lett.* **2010**, *104* (21), 216102.
(20) Morgenstern, K. Switching individual molecules by light and electrons: From isomerisation to chirality flip. *Prog. Surf. Sci.* **2011**, *86* (5−8), 115−161.
(21) Tallarida, N.; Rios, L.; Apkarian, V. A.; Lee, J. Isomerization of One Molecule Observed through Tip-Enhanced Raman Spectroscopy. *Nano Lett.* **2015**, *15* (10), 6386−94.
(22) Thomas, J. O.; Andrade, H. D.; Mills, B. M.; Fox, N. A.; Hoerber, H. J.; Faul, C. F. Imaging the Predicted Isomerism of Oligo(aniline)s: A Scanning Tunneling Microscopy Study. *Small* **2015**, *11* (28), 3430−4.

(23) Qiu, X. H.; Nazin, G. V.; Ho, W. Mechanisms of reversible conformational transitions in a single molecule. *Phys. Rev. Lett.* **2004**, *93* (19), 1 DOI: 10.1103/PhysRevLett.93.196806.
(24) Alemani, M.; Peters, M. V.; Hecht, S.; Rieder, K. H.; Moresco, F.; Grill, L. Electric field-induced isomerization of azobenzene by STM. *J. Am. Chem. Soc.* **2006**, *128* (45), 14446−7.
(25) Comstock, M. J.; Levy, N.; Kirakosian, A.; Cho, J.; Lauterwasser, F.; Harvey, J. H.; Strubbe, D. A.; Frechet, J. M.; Trauner, D.; Louie, S. G.; Crommie, M. F. Reversible photomechanical switching of individual engineered molecules at a metallic surface. *Phys. Rev. Lett.* **2007**, *99* (3), 038301.
(26) Morgenstern, K. Single molecule manipulation. *Surf. Interface Anal.* **2010**, *42* (10−11), 1634−1636.
(27) Morgenstern, K.; Lorente, N.; Rieder, K. H. Controlled manipulation of single atoms and small molecules using the scanning tunnelling microscope. *Phys. Status Solidi B* **2013**, *250* (9), 1671−1751.
(28) Simic-Milosevic, V.; Meyer, J.; Morgenstern, K. Chirality change of chloronitrobenzene on Au(111) induced by inelastic electron tunneling. *Angew. Chem., Int. Ed.* **2009**, *48* (22), 4061−4.
(29) Zhang, X.-m.; Xu, S.-d.; Li, M.; Shen, Y.-t.; Wei, Z.-q.; Wang, S.; Zeng, Q.-d.; Wang, C. Photo-Induced Polymerization and Isomerization on the Surface Observed by Scanning Tunneling Microscopy. *J. Phys. Chem. C* **2012**, *116* (16), 8950−8955.
(30) Guo, C.; Li, M.; Kang, S. Photochemical Reactions in Self-Assembled Organic Monolayers Characterized by using Scanning Tunneling Microscopy. *ChemPhysChem* **2016**, *17* (6), 802−11.
(31) Yadav, K.; Mahapatra, S.; Halbritter, T.; Heckel, A.; Gopakumar, T. G. Low-Threshold Reversible Electron-Induced and Selective Photoinduced Switching of Azobenzene Derivatives under Ambient Conditions. *J. Phys. Chem. Lett.* **2018**, *9* (21), 6326−6333.
(32) Kumagai, T.; Ladenthin, J. N.; Litman, Y.; Rossi, M.; Grill, L.; Gawinkowski, S.; Waluk, J.; Persson, M. Quantum tunneling in real space: Tautomerization of single porphycene molecules on the (111) surface of Cu, Ag, and Au. *J. Chem. Phys.* **2018**, *148* (10), 102330.
(33) Moresco, F.; Meyer, G.; Rieder, K. H.; Tang, H.; Gourdon, A.; Joachim, C. Conformational changes of single molecules induced by scanning tunneling microscopy manipulation: A route to molecular switching. *Phys. Rev. Lett.* **2001**, *86* (4), 672−675.
(34) Ladenthin, J. N.; Frederiksen, T.; Persson, M.; Sharp, J. C.; Gawinkowski, S.; Waluk, J.; Kumagai, T. Force-induced tautomerization in a single molecule. *Nat. Chem.* **2016**, *8* (10), 935−940.
(35) Huang, W.; Zhu, Z.; Wen, J.; Wang, X.; Qin, M.; Cao, Y.; Ma, H.; Wang, W. Single Molecule Study of Force-Induced Rotation of Carbon−Carbon Double Bonds in Polymers. *ACS Nano* **2017**, *11* (1), 194−203.
(36) Sader, J. E.; Jarvis, S. P. Accurate formulas for interaction force and energy in frequency modulation force spectroscopy. *Appl. Phys. Lett.* **2004**, *84* (10), 1801−1803.
(37) Bartels, L.; Meyer, G.; Rieder, K. H. Controlled vertical manipulation of single CO molecules with the scanning tunneling microscope: A route to chemical contrast. *Appl. Phys. Lett.* **1997**, *71* (2), 213−215.
(38) Hess, B.; Kutzner, C.; van der Spoel, D.; Lindahl, E. GROMACS 4: Algorithms for highly efficient, load-balanced, and scalable molecular simulation. *J. Chem. Theory Comput.* **2008**, *4* (3), 435−447.
(39) Bayly, C. I.; Cieplak, P.; Cornell, W. D.; Kollman, P. A. A Well-Behaved Electrostatic Potential Based Method Using Charge Restraints for Deriving Atomic Charges - the Resp Model. *J. Phys. Chem.* **1993**, *97* (40), 10269−10280.
(40) Wang, J. M.; Wolf, R. M.; Caldwell, J. W.; Kollman, P. A.; Case, D. A. Development and testing of a general amber force field. *J. Comput. Chem.* **2004**, *25* (9), 1157−1174.
(41) Heinz, H.; Vaia, R. A.; Farmer, B. L.; Naik, R. R. Accurate Simulation of Surfaces and Interfaces of Face-Centered Cubic Metals Using 12−6 and 9−6 Lennard-Jones Potentials. *J. Phys. Chem. C* **2008**, *112* (44), 17281−17290.
(42) Humphrey, W.; Dalke, A.; Schulten, K. VMD: Visual molecular dynamics. *J. Mol. Graphics* **1996**, *14* (1), 33−38.
(43) Kresse, G.; Furthmuller, J. Efficient iterative schemes for ab initio total-energy calculations using a plane-wave basis set. *Phys. Rev. B: Condens. Matter Mater. Phys.* **1996**, *54* (16), 11169−11186.
(44) Blochl, P. E. Projector Augmented-Wave Method. *Phys. Rev. B: Condens. Matter Mater. Phys.* **1994**, *50* (24), 17953−17979.
(45) Kresse, G.; Joubert, D. From ultrasoft pseudopotentials to the projector augmented-wave method. *Phys. Rev. B: Condens. Matter Mater. Phys.* **1999**, *59* (3), 1758−1775.
(46) Dion, M.; Rydberg, H.; Schröder, E.; Langreth, D. C.; Lundqvist, B. I. Van der Waals Density Functional for General Geometries. *Phys. Rev. Lett.* **2004**, *92* (24), 246401.
(47) Klimeš, J.; Bowler, D. R.; Michaelides, A. Chemical accuracy for the van der Waals density functional. *J. Phys.: Condens. Matter* **2010**, *22* (2), 022201.
(48) Klimeš, J.; Bowler, D. R.; Michaelides, A. Van der Waals density functionals applied to solids. *Phys. Rev. B: Condens. Matter Mater. Phys.* **2011**, *83* (19), 195131.

https://dx.doi.org/10.1021/jacs.0c00192
J. Am. Chem. Soc. 2020, 142, 10673−10680